3D-Printed 96 GHz Bull's-Eye Antenna with Off-Axis Beaming

Unai Beaskoetxea, Stefano Maci, *Fellow, IEEE*, Miguel Navarro-Cía, *Senior Member, IEEE*, and Miguel Beruete

***Abstract*— Reducing the profile, footprint and weight of antennas embarked on aircrafts, drones or satellites has been a long pursued objective. Here we tackle this issue by developing a millimeter-wave 96 GHz elliptical Bull's-Eye antenna with off-axis radiation at 16.5º that has been fabricated by low cost 3D printing stereolithography, followed by metal coating. The theoretical basis for optimum off-axis operations is explained. Measurement results show an overall good agreement with simulations, displaying a gain of 17 dB and a 3.5º beamwidth (E-plane) at the operational frequency. The off-axis beaming enlarges the potential applicability of this technology with respect to the broadside beam solution.**

***Index Terms*— Leaky wave horn antenna, off-axis beaming, stereolitography, bull's-eye antenna, corrugated surface, millimeter-waves**

I. Introduction

THE INCREASING data transfer volume driven by mobile communications, surveillance, and space-based navigation systems is rising wireless bandwidth demand on an unprecedented scale [1], [2]. To give solution to this growing exigence, engineers are moving into the millimeter-wave region [3]–[5]. In this range one may reduce the footprint and profile of high and medium gain antennas, resorting to a leaky-wave radiation mechanism [6]. This is particularly appealing for antennas mounted on unmanned aerial vehicles (UAV), microsatellites and cubeSats [7].

Leaky-wave antennas are classical radiating structures that have been known for a long time. Hansen, in 1946, patented a slitted electromagnetic waveguide capable of radiating a steerable beam [8]. Later, Oliner *et al.* studied the leakage of waveguides with different discontinuities along a side wall, performing a thorough analysis for uniform antennas [9], [10], and quasi-uniform antennas [11]. In parallel, modulated surfaces were analyzed for the propagation of surface and leaky waves in [12] and, soon after, for radiation from periodic structures [13]. Jackson, Guglielmi and other authors have presented the leaky-wave propagation and beam-scanning capabilities of diverse structures [14]–[16]. Nowadays, an extensive bibliography can be found on the subject [17]–[19].

Among the periodic structures, an interesting kind of antenna was reported in the microwave range as an evolution of the extraordinary optical transmission works developed in [20]–[22]. These antennas consist of a radiating slot surrounded by straight parallel [23]–[25] or annular concentric [26] corrugations. In the latter case, the structure is usually called Bull's-Eye (BE) antenna. BE antennas can be designed for broadside operation at a specific frequency. Due to the symmetry of the BE structure, they can also be designed to produce a conical-sector beam pattern within certain frequency range [27], although this pattern can also be achieved with a half BE [28].

The interpretation proposed in the optical regime was based on the coupling of the incident light to surface plasmon polaritons supported by the metal-air interface, excited thanks to the periodic structure milled on the metal [20]. Although this explanation was valid in that range given that the real part of the permittivity of metals is negative and comparable in magnitude to the permittivity of air, it was not completely accurate at lower frequency ranges, such as microwaves or millimeter-waves where metals are better described using a high conductivity approximation. Therefore, an alternative explanation was put in terms of the leaky-wave theory [29], [30], complementing the plasmonic interpretation. These antennas have been demonstrated at millimeter-waves for automobile radar [31] and space research applications [7] as well as in the terahertz [32] and mid-infrared band for quantum-cascade lasers [33].

In [16], [27], [34]–[36], a novel leaky wave Bull's Eye antenna design was analyzed thoroughly. Its novelty laid in that it consisted on a grounded dielectric slab (GDS) loaded with annular concentric metallic strips and fed by a coupled aperture slot along with a surface wave launcher. By means of this arrangement, the leakage of a TM_0 mode surface wave is achieved, in contrast to the TE_1 mode used in classical methodologies [14], [37], [38]. In addition, a technique to ensure efficient TM_0 radiation through the sectoring of the

[1]This work was supported by the Spanish Government under contract TEC2014-51902-C2-2-R. M. N.-C. is supported by University of Birmingham [Birmingham Fellowship]. M.B. acknowledges support by the Spanish Government under contract RYC-2011-08221.

U. Beaskoetxea, and M. Beruete are with the Antennas Group-TERALAB, Universidad Pública de Navarra, Pamplona 31006, Spain (e-mail: unai.beaskoetxea@unavarra.es; miguel.beruete@unavarra.es).

S. Maci is with the Department of Information Engineering, University of Siena, 50124 Siena, Italy (e-mail: macis@dii.unisi.it).

M. Navarro-Cía is with the School of Physics and Astronomy, University of Birmingham, Birmingham B15 2TT, UK (e-mail: m.navarro-cia@bham.ac.uk).

metallic grating to suppress the TE field distributions was presented. Previously, in [37], Encinar had presented a thorough analysis of the methods which permitted to obtain the fields in any region and the radiation characteristics of dielectric slabs loaded with metal strips, when the strip thickness was taken into account (mode matching method) or not (point matching method). Closer in time, the modal properties of the leaky and surface waves propagating along the metallic gratings on the GDS were scrupulously described in [39].

While clarifying the physical connection between the optical concept of holography and the leaky wave mechanism, a double period strip grating enabling off-broadside beaming was reported in 2007 [40]. Likewise in [41], [42] a thorough analysis was done about the beam sweeping capability of asymmetric structures based on subwavelength slits perforated in slabs surrounded by gratings at both sides. Tilted beams can be also obtained at lower frequencies with the use of metasurfaces made of subwavelength patches printed over a substrate [43], [44].

Taking as a basis the results of [45], different modifications of the symmetric Bull's Eye topology were studied for multiple discretely steerable beams [7]. Namely, a mechanically rotating plate containing a six-sector ring pattern placed over a central slot was proposed to obtain six different radiation angles for CubeSat applications [46]. In parallel to this work, but unrelated to the steering capabilities of the antenna, the increase of its directivity by the sole addition of a dielectric superstrate was proven in [47].

Here, motivated by the fast-prototyping and lightweight advantages provided by 3D printing technology, an off-axis BE antenna working at 96 GHz has been designed, fabricated and experimentally characterized. Although a similar antenna was presented in [48], design criteria were not disclosed in the above reference, and are re-interpreted here on the basis of a diffracted ray model. This asymmetric structure allows the antenna to radiate a steered beam in a direction governed by a forward (backward) interaction between the cylindrical wavefront of the wave launched by the feed and the annular corrugations in the upper (lower) part of the structure. Meanwhile, the stereolithography (SLA) 3D printing followed by chemical and electro-plating metallization offers a rapid and cost-effective fabrication solution of antennas, which easily includes the feed. The fabricated antenna presents a peak gain of 17 dB with a narrow beamwidth of approximately 3.5º in the E-plane. Experimental and numerical results show good agreement when fabrication tolerances are taken into account in the model. This structure offers a medium gain with the benefits of a reduced profile and a weight less than a fourth of a solid copper antenna.

The paper is organized as follows. Section II presents design formulas for the groove's design. Section III illustrates the details of the design procedure and the full wave simulations. Section IV presents the fabrication process and the experimental measurement. Section V concludes with a summary.

II. Formulation of the Groove Equations

In this section, we derive design equations for the curvilinear grooves to obtain an off-axis beam. With reference to Fig. 1, the upper half of the antenna (with $y > 0$) is designed to support a forward leaky-mode (from here on we will call *FW* to this part) and the lower half (*BW* part) is designed to support a backward leaky-mode. The grooves are designed so that at the operation frequency both parts of the aperture generate a beam in the same direction, see Fig. 1(b). In the following we describe the physical mechanism that leads to the design formulas.

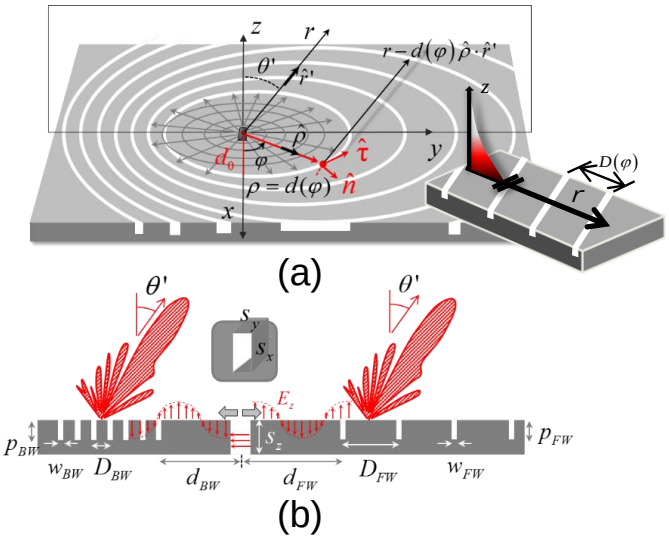

Fig. 1. Geometry. (a) 3D view (b) Cross-sectional view in the plane *y*-*z*, with detail of the rectangular waveguide feed and polarization of the electric field

The depth of the grooves is less than a quarter wavelength at the operation frequency and the width w (= w_{FW} = w_{BW}) is very small compared to the wavelength. Both parameters can be adjusted with different values in the *FW* and *BW* parts of the grooves to improve the antenna performance (p_{BW}, p_{FW} and w_{BW}, w_{FW}, depths and widths respectively).We assume that the structure is excited by an open ended waveguide centered at the origin of the reference system *x*-*y*-*z*. The observation point at the free-space interface is described by the cylindrical coordinates ρ, φ. The feed excites a grazing wave propagating with vertical electric field and cylindrical wavefront with free-space radial wavenumber $k = \omega\sqrt{\varepsilon_0\mu_0}$. Let us assume that the grazing wave can be described by radial rays at the first groove (Fig. 1(a)).

Consider first the coupling of the grazing wave with the curvilinear groove closest to the origin. We assume that the axis of this first groove is described by the polar coordinate equation $\rho = d(\varphi)$, where $\varphi \in (0º, 180º)$ for the *FW* part and $\varphi \in (180º, 360º)$ for the *BW* part of the aperture (see Fig. 1(a)).

Our goal is finding the analytical expression of the function $\rho = d(\varphi)$ for ensuring a phase-coherence condition for the scattered field from the first curvilinear groove in a direction $\hat{r}' = \cos\theta'\,\hat{z} + \sin\theta'\,\hat{y}$ (namely in a direction which forms an angle θ' with the *z*-axis in the plane *y*-*z*, see Fig. 1). To this

end, we can substitute the groove apertures with magnetic current rings radiating on top of the ground plane and fed by the grazing ray-field. The phase-matching conditions of scattered rays in direction $\hat{r}'$ can be formulated as:

$$kd(\varphi)+k[r-d(\varphi)\hat{\rho}\cdot\hat{r}']=kd_0+kr,\qquad \varphi\in(0,2\pi) \tag{1}$$

where r is the far field distance from the origin, $\hat{\rho}=\cos\varphi\hat{x}+\sin\varphi\hat{y}$ is the radial (ray) direction and $d_0=d(\varphi=0)$ is the distance of the first groove from the origin in the *x* direction. The term in the square brackets in (1) is the far field distance of a generic point of the ring in direction $\hat{r}'$ (see Fig. 1(a)). We note that (1) is valid in both *FW* and *BW* regions because of the sign inversion of the vertical electric field launched by the source in the two regions (see Fig. 1b). Since $\hat{\rho}\cdot\hat{r}'=\sin\theta'\sin\varphi$, we may rewrite (1) as:

$$d(\varphi)=\frac{d_0}{1-\sin\theta'\sin\varphi};\qquad \varphi\in(0,2\pi) \tag{2}$$

which defines the equation of the first groove as an ellipse with one focus at the origin. The intersection distance of the first groove with the *y* axis is obtained by substituting $\varphi=\pi/2$ and $\varphi=3\pi/2$ in (2). We denote this distance by d_{FW} and d_{BW}, respectively:

$$d_{FW}=d_0/(1-\sin\theta')\ ,\ d_{BW}=d_0/(1+\sin\theta') \tag{3}$$

The equations of the other magnetic current rings (grooves) can be calculated by assuming that the magnetic currents on all rings essentially depend on the incident field and not on the field scattered by the other grooves. Therefore, we can find their equations just setting $kd_0+2n\pi,\ n=0,1,2,..,$ in place of kd_0 in the second member of (1). This implies that all rings radiate in phase with the first ring (n = 0). This leads to:

$$d^{(n)}(\varphi)=\frac{d_0+n\lambda}{1-\sin\theta'\sin\varphi}\ ,\ n=0,1,2,..P \tag{4}$$

where λ is the free space wavelength and by definition $d^{(0)}(\varphi)\equiv d(\varphi)$. Equation (4) represents the equations of confocal ellipses with one focus at the origin. Note that in the *FW* region sinφ is positive, and then the interspace between grooves, represented by $D(\varphi)=\lambda/(1-\sin\theta'\sin\varphi)$, is larger than the wavelength, while in the *BW* region sinφ is negative and the groove interspace is less than a wavelength. In particular, for $\varphi=\pi/2$ and $\varphi=3\pi/2$ we obtain, respectively, the following interspaces:

$$D_{FW}=\lambda/(1-\sin\theta');\quad D_{BW}=\lambda/(1+\sin\theta') \tag{5}$$

Equation (5) has an interesting interpretation. Let us denote by $\hat{n}$ and $\hat{\tau}$, the unit vector normal and tangent to $\rho=d(\varphi)$ at each point $P\equiv(\rho,\varphi)$, respectively (see Fig. 1(a)). Imagine that the aperture domain is decomposed into angular sectors of elementary angular aperture $d\varphi$, each sector fed by a grazing ray-field propagating along $\hat{\rho}$. The magnetic currents that represent each groove can be locally thought of as obtained from the interaction between a local planar wavefront and 1D rectilinear oblique grooves locally tangent to the curvilinear grooves, and with local period along $\hat{\rho}$ given by $D(\varphi)$. The latter is a sort of local "canonical" problem to which we may attribute a generalized Floquet-wave expansion with dominant (0-indexed) local wavevector given by $k\hat{\rho}$. The other wavevectors of this local expansion can be found as follows. First, one projects $k\hat{\rho}$ along the two directions $\hat{n}$ and $\hat{\tau}$. The component along $\hat{\tau}$ is preserved along the ray-path, while the component along $\hat{n}$ is affected by the local periodicity $D(\varphi)$ and therefore by a periodic shift equal to $2\pi m/\left[D(\varphi)\hat{n}\cdot\hat{\rho}\right]$; m=0, ±1, ±2.. . The dominant LW local wavevector $\boldsymbol{\beta}_{LW}$ is obtained by setting $m=-1$, which is the only spatial harmonic inside the visible region. This procedure leads to

$$\boldsymbol{\beta}_{LW}=k(\hat{\rho}\cdot\hat{\tau})\hat{\tau}+\left[k(\hat{\rho}\cdot\hat{n})-\frac{2\pi}{D(\varphi)\hat{n}\cdot\hat{\rho}}\right]\hat{n}=k\hat{\rho}-\frac{2\pi\hat{n}}{D(\varphi)\hat{n}\cdot\hat{\rho}} \tag{6}$$

Introducing in the above equation the value $D(\varphi)=\lambda/(1-\sin\theta'\sin\varphi)$ and the analytical expression of $\hat{n}$:

$$\hat{\mathbf{n}}=\nabla_t\left[\rho(1-\sin\theta'\sin\varphi)\right]/\left|\nabla_t\left[\rho(1-\sin\theta'\sin\varphi)\right]\right| \tag{7}$$
$$=\left[\hat{\boldsymbol{\rho}}(1-\sin\theta'\sin\varphi)-\hat{\boldsymbol{\varphi}}\sin\theta'\cos\varphi\right]/\sqrt{(1-\sin\theta'\sin\varphi)^2+(\sin\theta'\cos\varphi)^2}$$

it can be easily shown that (6) implies $\boldsymbol{\beta}_{LW}=k\sin\theta'\,\hat{y}$.

This means that the direction of the local LW wavevector is independent of φ for all the angular sector, and therefore define a global linear phasing of the aperture along the direction *y*. In the interpretation we have just described, the angular sectors relevant to $y<0$ and $y>0$ contribute with local backward and forward local leaky modes contributions, respectively.

III. Prototype Design And Simulation Results

For a complete characterization of the antenna, the whole structure was designed and studied using the commercial software CST Microwave Studio™ [49]. A magnetic symmetry was defined in the *y-z* plane to reduce the computational effort. The optimized parameters are summarized in Table I.

The grooves have been designed using (4). The open ended waveguide cross section, hereinafter simply denoted by slot, has the next parameters: s_x = 1.627 mm × s_y = 0.470 mm; the slot depth is s_z = 0.77 mm perforated on a metallic 74 mm × 71

mm slab, fed by a WR-10 standard waveguide fixed on the rear part. This slot permits the coupling of the power to a transverse magnetic (TM, with H field normal to *z*) surface wave, which propagates along the metal-air interface, through the transversal resonance determined by its width. The arbitrary constant d_0 as well as the grooves' width and depth for both *FW* and *BW* regions were obtained by means of an optimization routine, based on the Trust Region Framework, setting as a goal achieving the highest possible gain at $\theta' = 15°$ and as low side lobe level as possible at the design frequency. Due to the asymmetry of the antenna, the optimization routine for the groove's dimensions took into account the possibility of different widths and depths. Based on previous works, $\lambda/7$ was chosen as a seed for both width and depth at both sides. The optimization, which returned values between $\lambda/6$ and $\lambda/8$, is essential for a maximum gain at the design wavelength, given that a slight variation of the grooves' dimensions may lead to a shift of the frequency of the maximum radiation. Thus, both the period of the corrugations and their dimensions must be chosen adequately to obtain the largest gain at the frequency of design.

TABLE I
PARAMETER VALUES (OPERATING FREQUENCY 93GHz)

Para-meter	Description	Value (μm)	Value (λ)
d_{FW} [1]	Forward Offset	4501	1.44
d_{BW} [1]	Backward Offset	2650	0.85
D_{FW} [2]	Forward Period	4142	1.33
D_{BW} [2]	Backward Period	2438	0.78
s_x	Slot Width	1627	0.52
s_y	Slot Height	470	0.15
s_z	Slot Depth	770	0.25
p_{FW}	Forward Grooves' Depth	520	0.17
p_{BW}	Backward Grooves' Depth	500	0.16
w_{FW}	Forward Grooves' Width	510	0.16
w_{BW}	Backward Grooves' Width	420	0.13
d_0	Intersection distance with *x*	3189	0.99
H	Slab Height	74066	23.70
L	Slab Width	71139	22.76

[1] Offset goes from slot center to groove center.
[2] Period goes from groove center to groove center. $n \neq 1$

In this case, the optimized groove dimensions excite predominantly the TE_{11} mode (referred to the fundamental mode of the coaxial waveguide that can be associated to each groove). If wider corrugations were employed, the first higher order mode (TM_{11}) could be also excited [50]. However, this option was discarded as the wide corrugations at the lower half merged into a single cavity due to their proximity. A non-uniform hexahedral mesh with smallest mesh cell of 44 μm × 32 μm × 127 μm (13.66λ × 9.93λ × 39.40λ) was used to map accurately the geometry.

The number of rings was chosen as a good tradeoff between size, gain and side lobe level, as explained next. A simulation study has been performed to observe the evolution of the gain with the number of rings from $P = 0$ to 8. The results presented in Fig. 2(a) demonstrate that a higher gain as well as a narrower bandwidth is obtained as more rings are added to the grating. The gain increment is reduced when *P* increases, due to the fact that the field is almost completely radiated when it arrives at the peripheral ring. Thus, as observed in [23], at a sufficiently large number of periods, the increase of the gain for consecutive number of grooves will be negligible. This was also reported in [26] and very recently in [31].

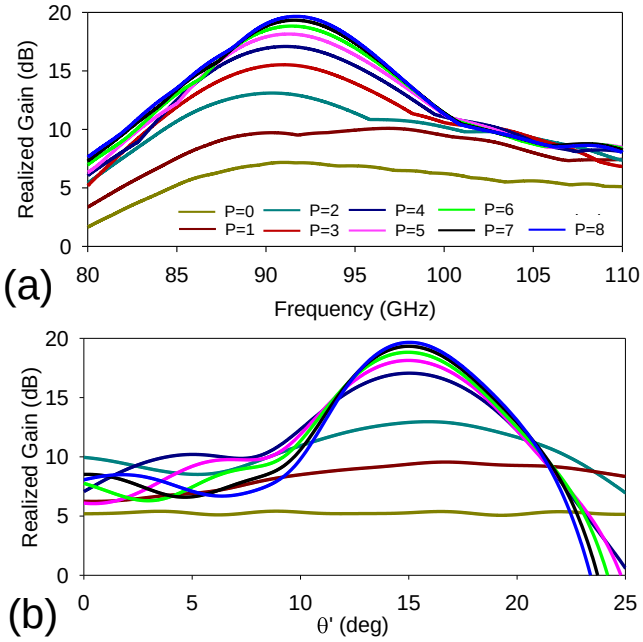

Fig. 2. Realized gain vs frequency at $\theta' = 15°$ (a) and E-plane radiation pattern at $f = 91.6$ GHz as the number of periods is increased from $P = 0$ to $P = 8$ (b).

Fig. 2(b) displays a detail of the evolution of the E-plane diagram, from $\theta' = 0°$ to $\theta' = 25°$, with *P*. Remarkably, with just $P = 2$ the antenna shows a beam around $\theta' = 15°$, in comparison with the near isotropic radiation of a non-corrugated structure ($P = 0$), and as the number of periods is increased, both the beamwidth and the side lobe level are reduced. Notice that although $P = 8$ has the higher gain, its side lobe level is slightly worse than $P = 7$. Hence, the choice of $P = 7$ for the prototype.

Fig. 3 presents simulation and measurements (commented in the following sections) for the antenna with seven rings. The blue curve in Fig. 3(a) corresponds to the simulated return loss of the ideal structure, which presents a dip at ~93 GHz (the other curves will be commented in the next section). The location of the minimum return loss is governed by the transversal resonance fixed by the slot width, s_x, which is approximately half the operating wavelength at $f = 93$ GHz ($\lambda = 3.22$ mm) and its depth depends on the slot's height s_y. Blue curves in Fig. 3(b, c) represent the realized gain and the E-plane (*y*-*z* plane) radiation diagram at $f = 91.6$ GHz, which is the frequency of maximum gain, respectively. As it is shown, the simulated ideal antenna presents a peak gain of 19.3 dB at the design frequency and the maximum radiation points towards 15º. It has a relatively narrow –3dB beamwidth $\theta'_{-3dB} = 5.1°$ and the side lobe (appearing as a slight shoulder at 0.5º) level is near –10.8 dB.

The H-plane radiation pattern at $f = 91.6$ GHz (elevation angle $\theta' = 15°$) is displayed in Fig. 3(d). The corresponding

beamwidth in this plane is φ'_{-3dB} = 10.2º, and the cross level value is at least –23.2 dB within this beamwidth. Needless to say, the magnetic symmetry of the structure in the *y*-*z* plane, corresponding to the E-plane, imposes a null of cross-polar at φ' = 0º. The cross-polar observed for the H-plane can be assigned to the TE_{11} mode excited in the grooves that possess E_x (and E_y) components.

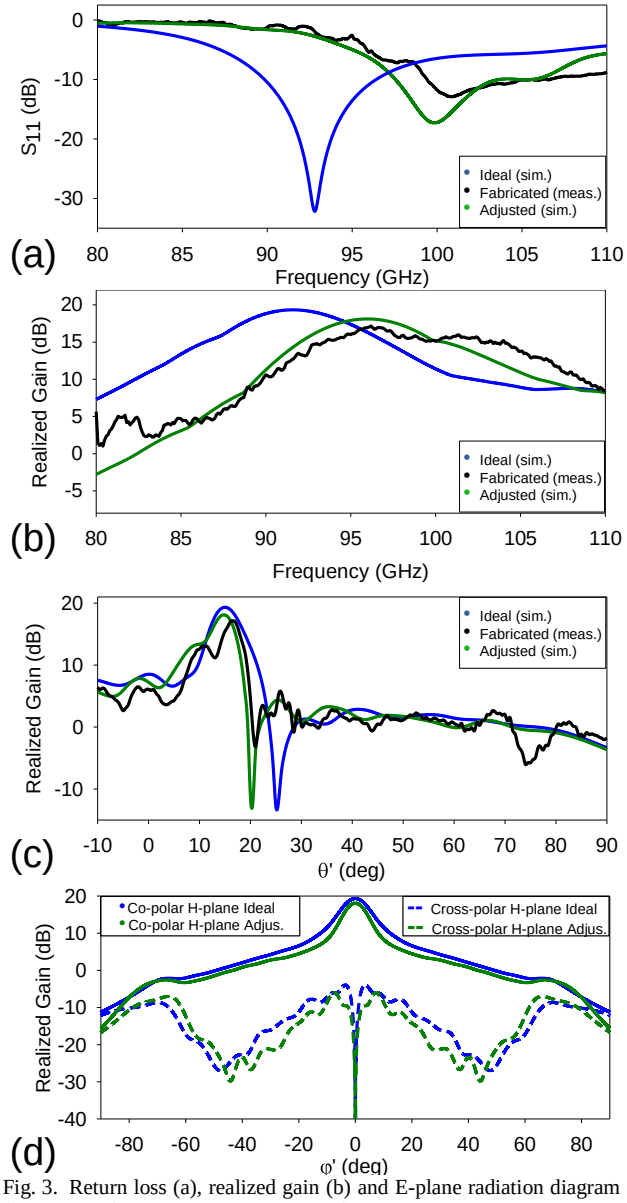

Fig. 3. Return loss (a), realized gain (b) and E-plane radiation diagram at the frequency of the maximum gain (c) for the simulated ideal (blue curves), experimentally measured (black curves) and simulated adjusted (green curves) antenna. Co-polar (continuous line) and cross-polar (dashed line) H-plane radiation diagrams at the frequency of the maximum gain for simulated ideal (blue curves) and adjusted (green curves) antennas (d).

As it can be seen in Fig. 4(a), the current density is higher in the vertical direction, corresponding to the E-plane. Thus, this antenna presents a higher leaky wave radiation contribution for this plane (Fig. 4(b)). Regarding the aperture efficiency, as expected for this kind of antennas, a low value of slightly more than e_a = 6% is obtained.

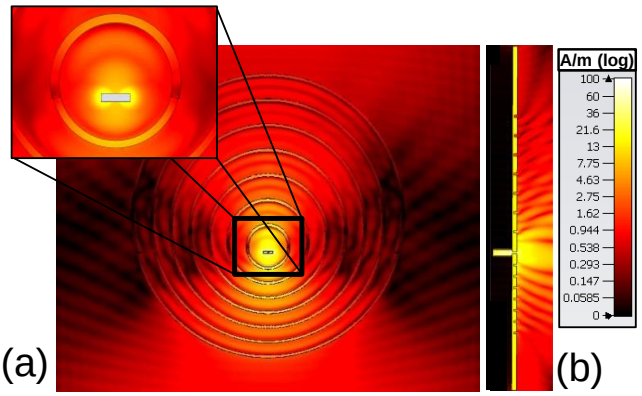

Fig. 4. Surface current magnitude distribution in plane *x*-*y* (a) and near-H_x-field in plane *y*-*z* (b) at *f* = 91.6 GHz. Inset: detail of the slot and first ring.

Fig. 5(a) presents contour plots showing the simulated realized gain as a function of frequency and angle in the E-plane (Figs. 5(b, c) will be commented in the next section). It can be seen that from 91 to 96 GHz, the antenna presents a maximum gain exceeding 18 dB with a narrow beam (θ'_{-3dB} ~ 5º) pointing at 15º and side lobe level larger than 10 dB out of the 90 GHz - 92.5 GHz range though. It is also interesting to observe that, inverting (5), the equation which governs the beam direction θ', in the E-plane is given by:

$$\sin\theta' = 1 - \lambda / D_{FW};\ \sin\theta' = \lambda / D_{BW} - 1 \qquad (8)$$

By fixing D_{FW} and D_{BW} two sets of curves are obtained by means of (8) as a function of frequency, that are represented in Fig. 5(a-c) as white and black dashed lines for D_{FW} and D_{BW} respectively. These curves identify the pointing angles relevant to the *FW* and *BW* part of the antenna when changing frequency. They cross approximately at the operating frequency and beam direction.

By means of (6) the phase constant is both analytically and numerically obtained. Fig. 6 presents a comparison of the numerically computed (red curves) and simulated (blue curves) beam directions as a function of the phase constant β for *FW* (continuous curves) and *BW* (dashed curves) parts. A good agreement can be observed for the forward leaky mode. The backward leaky mode shows, however, a slight frequency shift between theory and simulation that we attribute to a combination of numerical error (mainly, originated from the meshing) and antenna finite size effect.

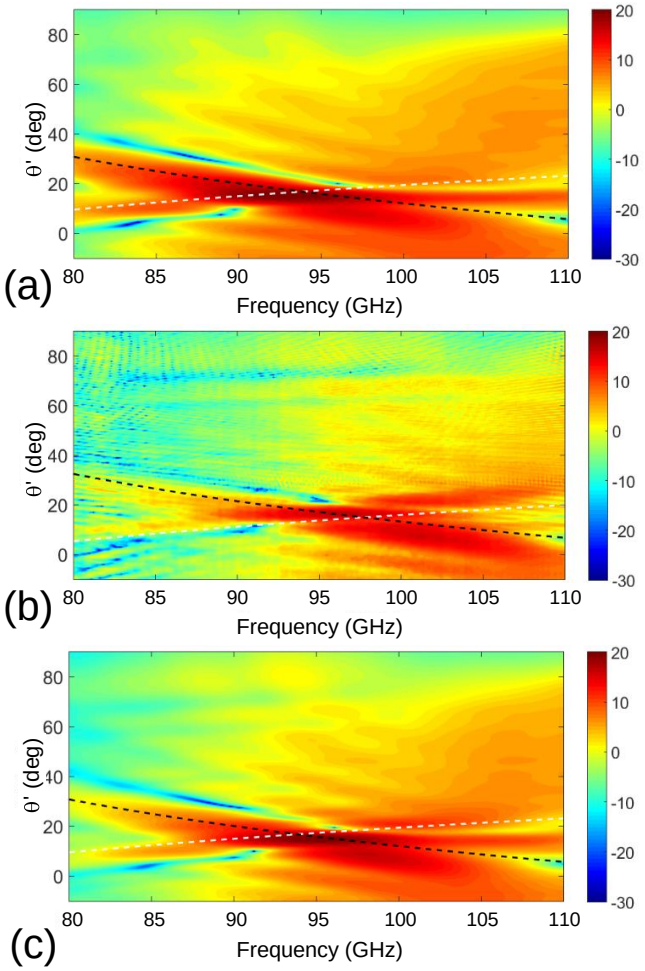

Fig. 5. Realized gain in dB for E-plane: simulation for the ideal antenna (a), measurements (b) and simulations for the adjusted antenna (c). Black and white dashed curves correspond to the analytically calculated θ' direction vs. frequency for the beam radiated by the *BW* and *FW* part, respectively.

For the sake of completeness, the attenuation constant α was also obtained for both *FW* and *BW* halves. For this, two 1D corrugated antennas, one with the parameters of *FW* and the other one with the ones of *BW* part, were simulated. Then, the attenuation constant was calculated by applying the generalized pencil-of-function (GPOF) method [51] to the decaying H_x field observed along the propagating surfaces in the *y* direction, once the contribution of the flat surface (inversely proportional to the square root of the distance) was subtracted. With this method we obtained $\alpha/k = 0.026$ and $\alpha/k = 0.041$ for the *FW* and *BW* sections at $f \sim 92$ GHz, respectively. In order to validate these results, these values of the attenuation constant were introduced in the next equation:

$$\theta_{-3dB} = \frac{2\alpha}{k}\cos(\theta') \qquad (9)$$

where θ_{-3dB} is the width of the beam observed for the simulated 1D structures at the pointing angle θ' and k is the free-space radial wavenumber. The semi-analytical beamwidth and the beamwidth obtained directly from the far field simulation were in very good agreement: 3.05º for the *FW* part and 4.63º for the *BW* part. The simulated structures consisted of 50 periods so as to avoid reflections at the edge of the structure, which thwart the extraction of α by means of the GOPF method. In addition, the equation in (9) is only valid for a periodic structure for which the propagating power remaining on the surface is negligible, which in practical terms is equivalent to a very long structure. However, these values allow us to gain an overall view of the behavior of the 7 period structures.

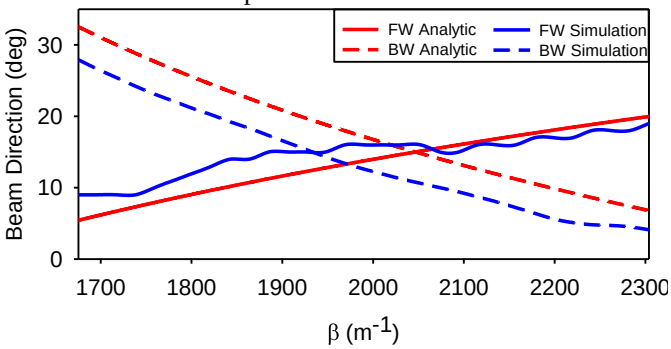

Fig. 6. Numerically computed (red curves) and simulated (blue curves) beam directions as a function of the phase constant for *FW* (continuous curves) and *BW* (dashed curves) parts.

IV. Fabrication and Experimental Measurements

The antenna was printed in a SLA 3D Systems Viper™ machine, based on the layer-by-layer solidification of a photo reactive resin by means of an ultraviolet light beam. The 3D printed split-block antenna can be seen in Fig. 7. To minimize radiation losses, the juncture was along the E-plane [52]. Once each half of the antenna was obtained and properly cured, they underwent a four stage chemical process to make them conductive with an electro-less nickel layer, over which a copper layer 30 μm thick (conductivity $\sigma = 5.8\times10^7$ S/m) was deposited using an electro-plating process. Then, the metallized halves were fastened by means of screws. The fabricated antenna was weighed using a JT-120M Cobos precision balance. The total weight of the final structure was 111.2 g, of which 50.95 g corresponded to the fasteners. In comparison, a solid copper antenna would weight ~ 456 g (estimation based on copper's density, 8.9 g/cm^3). Thus, an antenna with a weight less than 75% of a solid metal antenna is obtained.

Fig. 7(a, b) show a half uncoated antenna and the metallized antenna, as well as a side view of the flange for both structures. The antenna's dimensions were then measured by means of a Mitutoyo 176-206D electronic microscope in order to quantify the differences introduced due to the fabrication tolerances. Figs. 7(c-e) display a detail of the front view, the slot and the intersection between upper and lower corrugations, respectively. The largest differences were found for the slot and grooves' width, presenting a ~1500 μm slot and ~160 μm narrower grooves (350 μm for the *FW* region and 260 μm for the *BW* region). A new series of simulations were subsequently launched incorporating the measured parameters in order to have a more accurate correlation between numerical and experimental results. This corrected design will be referred to in the following as "adjusted" antenna.

The radiation characteristics of the antenna were experimentally obtained by an ABmm^{TM} Quasioptical Vector Network Analyzer (VNA). First, in order to obtain the return loss, the BE was connected to a directional coupler and calibrated by blocking the slot with a metallic plane at the output so as to record the maximum reflection. Then, once the short-circuit was removed, the reflection was measured.

As it can be seen in Fig. 3(a), the measurements (black curve) and simulated adjusted (green curve) results have a good agreement. Both present a frequency shift with respect to the ideal geometry (blue curve) simulation, due to the aforementioned fabrication errors. As expected, a narrower slot leads to a S_{11} response shifted towards higher frequencies.

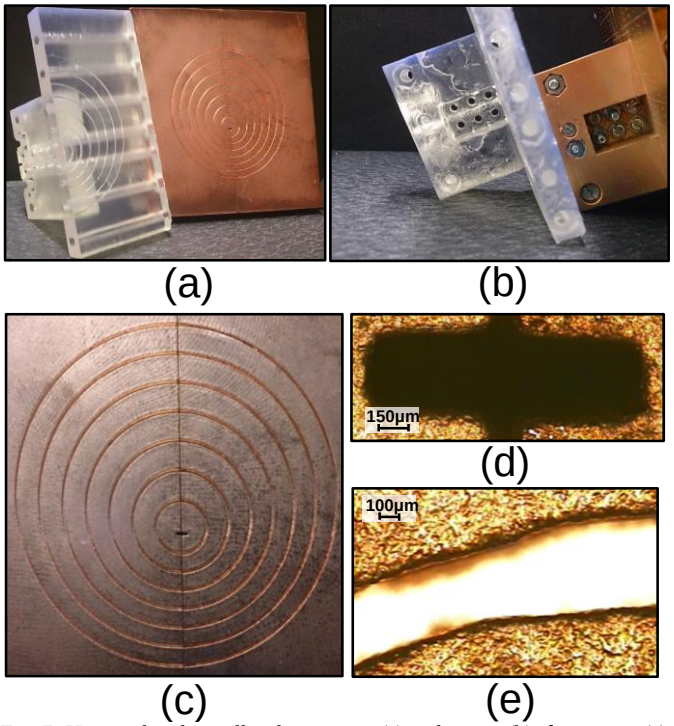

Fig. 7. Uncoated and metallized structures (a), side view (b), front view (c). Microscope pictures showing a detail of slot (d) and a detail of the intersection of *BW* and *FW* corrugations (e).

E-plane radiation pattern measurements were also carried out. Two opposite platforms were placed at a distance of 4.5 m (due to instrumentation constraints, this value is below the farfield condition which is near 6.5 m), on which the BE antenna and a W-band (WR-10 standard) horn antenna were placed and carefully aligned. The antenna under test was mounted over a software controllable rotary platform, which permitted azimuth sweeping. Both antennas' centers were 1.10 m above the floor and 1.50 m below the ceiling. Both antennas were connected to the VNA. To avoid spurious reflections, the path and the antenna test equipment were covered with radar absorbing material. The calibration was done by removing the antenna and placing another W-band test horn antenna as the emitter and recording the free-space transmission versus frequency. This curve served as a base for the measurement, allowing the cancellation of the frequency dependent response introduced by the system.

The E-plane radiation diagram for the BE antenna was acquired from −10 to 90º, with a step of 0.5º, and from 80 to 110 GHz with a step of 100 MHz. Black curves in Fig. 3 show the recorded realized gain (Fig. 3(b)) and E-plane radiation diagram (Fig. 3(c)), whereas green curves show values for the adjusted antenna. The H-plane was not experimentally characterized because, as discussed above, the leaky wave responsible for the enhanced radiation and tilted beaming runs along the vertical direction modifying fundamentally the E-plane diagram (in fact, the antenna is designed to have a tilted beam only in the E-plane). Hence, the H-plane of the simulated ideal antenna is only compared with that of the simulated adjusted antenna (Fig. 3(d)).

As it was commented in Section III, due to the narrowing of the corrugations in the manufactured prototype, a 4 GHz shift of the maximum gain frequency towards 96 GHz appears for both manufactured and adjusted antennas. This deviation from the optimal values causes a reduction of approximately 1 dB in the gain, according to the simulation results of the adjusted antenna. The experimental gain presents a reduction of ~2.3 dB (the peak gain reaches 17 dB), which might be due to the extra losses introduced by metal roughness [52] and additional experimental errors not considered in the simulation. Furthermore, there is a slight deviation of approximately 1.5º in the pointing angle of the θ'_{-3dB} = 3.5º beam that happens in the experiment at θ' = 16.5° instead of the design value of 15º, attributable to misalignment of the antennas in the experimental setup.

Following a similar process to that carried out for the ideal antenna, the attenuation constants at f = 96 GHz were calculated for the fabricated antenna. Thus, for the *FW* section it was obtained α/k = 0.02, whereas for the *BW* section α/k = 0.017. The lower values of α/k for the fabricated antenna verify the observed narrower experimental beamwidth compared to that of the ideal antenna. This highlights that the fabrication tolerances affect in a higher degree the *BW* half, as the deviation between the normalized attenuation constants for *BW* is evidently larger than for *FW*. In this case, the simulated beamwidth for the *FW* part (2.36º) and the theoretical one obtained with (9) (2.33º) agree in a higher degree than the simulated and theoretical values for the *BW* part (2.27º and 2º, respectively).

The experimental contour plot showing the E-plane gain in terms of frequency and angle at the previously specified ranges is displayed in Fig. 5(b). It shows an overall good agreement with the simulated ideal geometry (Fig. 5(a)) and adjusted geometry (Fig. 5(c)), aside from the mentioned frequency shift and reduced gain due to fabrication tolerances.

V. Conclusion

An asymmetric leaky-wave Bull's-Eye antenna working at 96 GHz has been designed, fabricated and experimentally characterized. The asymmetric distribution of the half-annular corrugations in the upper and lower half of the antenna enables a tilted beam pointing at 16.5º. Simple design formulas for the grooves' shape have been presented. The

optimized design has been described and then the 3D printed split-block antenna has been fabricated by stereolithography, copper-coated and then fastened. The results obtained for the ideal and fabricated antennas agree quite well, except for a frequency shift in both the S_{11} matching frequency and in the frequency of maximum gain. This shift is arguably due to fabrication tolerances, since introducing the realized values in the model the frequency shift has been recovered. The fabricated antenna presents, at the operation frequency f = 96 GHz, a 17 dB gain and a -3dB beamwidth in the E-plane of 3.5º at a beam pointing angle θ' = 16.5º. Despite the slight inaccuracies and the high-operating frequency, the present solution provides an effective alternative to fully metal structures, thanks to its cost-effective fabrication process and the 75% weight reduction. Although the tolerances on each fabrication step are somehow known a priori and were taken into account in the design, the overall fabrication tolerance is not. This is the origin of the shifts observed in this work in both pointing angle and input-impedance bands with respect to the beamwidth and bandwidth, respectively. As far as design and fabrication are concerned, a closed-loop dimensional control process should be carried out to produce an optimized prototype. This kind of antennas may be interesting for UAV and microsatellite applications and in high-capacity point-to-point communications which require a tilted beam.

ACKNOWLEDGMENT

The authors would like to thank 3DDC Ltd for the manufacturing of the SLA printed parts and the copper plating and to Dr. Mario D'Auria for fruitful discussion at the prototyping stage.

REFERENCES

[1] T. Kleine-Ostmann and T. Nagatsuma, "A review on terahertz communications research," *J. Infrared, Millimeter, Terahertz Waves*, vol. 32, no. 2, pp. 143–171, 2011.

[2] R. Q. Shaddad, A. B. Mohammad, S. A. Al-Gailani, A. M. Al-hetar, and M. A. Elmagzoub, "A survey on access technologies for broadband optical and wireless networks," *J. Netw. Comput. Appl.*, vol. 41, pp. 459–472, 2014.

[3] C. H. Doan, S. Emami, A. M. Niknejad, and R. W. Brodersen, "Millimeter-wave CMOS design," *IEEE J. Solid-State Circuits*, vol. 40, no. 1, pp. 144–154, 2005.

[4] N. Gopalsami and A. C. Raptis, "Millimeter-wave radar sensing of airborne chemicals," *IEEE Trans. Microw. Theory Tech.*, vol. 49, no. 4, pp. 646–653, 2001.

[5] W. Roh, J. Y. Seol, J. Park, B. Lee, J. Lee, Y. Kim, J. Cho, K. Cheun, and F. Aryanfar, "Millimeter-wave beamforming as an enabling technology for 5G cellular communications: Theoretical feasibility and prototype results," *IEEE Commun. Mag.*, vol. 52, no. 2, pp. 106–113, 2014.

[6] D. R. Jackson, C. Caloz, and T. Itoh, "Leaky-Wave Antennas," *Proc. IEEE*, vol. 100, no. 7, pp. 2194–2206, Jul. 2012.

[7] C. J. Vourch and T. D. Drysdale, "V-Band 'Bull's Eye' Antenna for CubeSat Applications," *IEEE Antennas Wirel. Propag. Lett.*, vol. 13, pp. 1092–1095, 2014.

[8] W. W. Hansen, "Radiating Electromagnetic Waveguide," U.S. Patent 2402622, 1946.

[9] L. Goldstone and A. Oliner, "Leaky wave antennas II: Circular waveguides," *IRE Trans. Antennas Propag.*, vol. 9, no. 3, pp. 280–290, 1961.

[10] A. A. Oliner, "Uniform Waveguide Leaky Wave Antennas," in *Proceedings of SPIE, Millimeter Wave Technology III*, 1985, vol. 544.

[11] L. O. Goldstone and A. A. Oliner, "Leaky-Wave Antennas I: Rectangular Waveguides," *IRE Trans. Antennas Propag.*, vol. 7, no. 4, 1959.

[12] A. A. Oliner and A. Hessel, "Guided waves on sinusoidally-modulated reactance surfaces," *IRE Trans. Antennas Propag.*, vol. 7, no. 5, pp. 201–208, Dec. 1959.

[13] R. A. Sigelmann and A. Ishimaru, "Radiation from periodic structures excited by an aperiodic source," *IEEE Trans. Antennas Propag.*, vol. 13, pp. 354–364, 1965.

[14] M. Guglielmi and D. R. Jackson, "Broadside Radiation from Periodic Leaky- Wave Antennas," *IEEE Trans. Antennas Propag.*, vol. 41, no. 1, pp. 31–37, 1993.

[15] G. Lovat, P. Burghignoli, and D. R. Jackson, "Fundamental Properties and Optimization of Broadside Radiation From Uniform Leaky-Wave Antennas," *IEEE Trans. Antennas Propag.*, vol. 54, no. 5, pp. 1442–1452, May 2006.

[16] S. K. Podilchak, P. Baccarelli, P. Burghignoli, A. P. Freundorfer, and Y. M. M. Antar, "Analysis and Design of Annular Microstrip-Based Planar Periodic Leaky-Wave Antennas," *IEEE Trans. Antennas Propag.*, vol. 62, no. 6, pp. 2978–2991, 2014.

[17] C. H. Walter, *Traveling Wave Antennas*. McGraw Hill, 1965.

[18] A. A. Oliner and D. R. Jackson, "Leaky-Wave Antennas," in *Antenna Engineering Handbook*, Mc Graw-Hi., J. L. Volakis, Ed. New York: Mc Graw-Hill, 2007, pp. 11–1/11–56.

[19] F. Monticone and A. Alù, "Leaky-Wave Theory, Techniques, and Applications: From Microwaves to Visible Frequencies," *Proc. IEEE*, vol. 103, no. 5, pp. 793–821, 2015.

[20] H. J. Lezec, A. Degiron, E. Devaux, R. A. Linke, L. Martin-Moreno, F. J. Garcia-Vidal, and T. W. Ebbesen, "Beaming light from a subwavelength aperture," *Science*, vol. 297, no. 5582, pp. 820–822, Aug. 2002.

[21] M. Beruete, I. Campillo, J. S. Dolado, J. E. Rodríguez-Seco, E. Perea, and M. Sorolla, "Enhanced microwave transmission and beaming using a subwavelength slot in corrugated plate," *IEEE Antennas Wirel. Propag. Lett.*, vol. 3, no. 1, pp. 328–331, Dec. 2004.

[22] M. Beruete, M. Sorolla, I. Campillo, and J. S. Dolado, "Subwavelength slotted corrugated plate with enhanced quasioptical millimeter wave transmission," *IEEE Microw. Wirel. Components Lett.*, vol. 15, no. 4, pp. 286–288, Apr. 2005.

[23] M. Beruete, I. Campillo, J. S. Dolado, E. Perea, F. Falcone, and M. Sorolla, "Dual-band low-profile corrugated feeder antenna," *IEEE Trans. Antennas Propag.*, vol. 54, no. 2, pp. 340–350, 2006.

[24] M. Beruete, I. Campillo, J. S. Dolado, J. E. Rodríguez-Seco, E. Perea, F. Falcone, and M. Sorolla, "Low-Profile Corrugated Feeder Antenna," *IEEE Antennas Wirel. Propag. Lett.*, vol. 4, no. 1, pp. 378–380, 2005.

[25] M. Beruete, I. Campillo, J. S. Dolado, J. E. Rodríguez-Seco, E. Perea, F. Falcone, and M. Sorolla, "Very Low Profile and Dielectric Loaded Feeder Antenna," *IEEE Antennas Wirel. Propag. Lett.*, vol. 6, no. 99, pp. 544–548, 2007.

[26] M. Beruete, I. Campillo, J. S. Dolado, E. Perea, F. Falcone, and M. Sorolla, "Very Low-Profile 'Bull' s-Eye' Feeder Antenna," *IEEE Antennas Wirel. Propag. Lett.*, vol. 4, no. 2, pp. 365–368, 2005.

[27] S. K. Podilchak, P. Baccarelli, P. Burghignoli, A. P. Freundorfer, and Y. M. M. Antar, "Optimization of planar periodic leaky-wave antennas by selective surface-wave suppression," *8th Eur. Conf. Antennas Propagation, EuCAP 2014*, pp. 770–774, 2014.

[28] S. K. Podilchak, A. P. Freundorfer, and Y. M. M. Antar, "Planar

Leaky-Wave Antenna Designs Offering Conical-Sector Beam Scanning and Broadside Radiation Using Surface-Wave Launchers," *IEEE Antennas Wirel. Propag. Lett.*, vol. 7, pp. 155–158, 2008.

[29] D. R. Jackson, A. A. Oliner, T. Zhao, and J. T. T. Williams, "Beaming of light at broadside through a subwavelength hole: Leaky wave model and open stopband effect," *Radio Sci.*, vol. 40, no. 6, pp. 1–12, Dec. 2005.

[30] A. Sutinjo and M. Okoniewski, "A Simple Leaky-Wave Analysis of 1-D Grooved Metal Structure for Enhanced Microwave Radiation," *IEEE Trans. Antennas Propag.*, vol. 60, no. 6, pp. 2719–2726, Jun. 2012.

[31] U. Beaskoetxea, V. Pacheco-Peña, B. Orazbayev, T. Akalin, S. Maci, M. Navarro-Cía, and M. Beruete, "77 GHz High Gain Bull's-Eye Antenna With Sinusoidal Profile," *IEEE Antennas Wirel. Propag. Lett.*, vol. 14, pp. 205–208, 2015.

[32] M. Beruete, U. Beaskoetxea, M. Zehar, A. Agrawal, S. Liu, K. Blary, A. Chahadih, X.-L. Han, M. Navarro-Cía, D. Etayo, A. Nahata, T. Akalin, and M. Sorolla, "Terahertz Corrugated and Bull's-Eye Antennas," *IEEE Trans. Terahertz Sci. Technol.*, vol. 3, no. 6, pp. 740–747, Nov. 2013.

[33] N. Yu, J. Fan, Q. J. Q. J. Wang, C. Pflügl, L. Diehl, T. Edamura, M. Yamanishi, H. Kan, and F. Capasso, "Small-divergence semiconductor lasers by plasmonic collimation," *Nat. Photonics*, vol. 2, no. 9, pp. 564–570, Jul. 2008.

[34] P. Baccarelli, P. Burghignoli, G. Lovat, and S. Paulotto, "A novel printed leaky-wave 'bull-eye' antenna with suppressed surface-wave excitation," in *IEEE Antennas and Propagation Society Symposium, 2004.*, 2004, vol. 1, pp. 1078–1081.

[35] S. K. Podilchak, P. Baccarelli, P. Burghignoli, A. P. Freundorfer, and Y. M. M. Antar, "Optimization of a Planar 'Bull-Eye' Leaky-Wave Antenna Fed by a Printed Surface-Wave Source," *IEEE Antennas Wirel. Propag. Lett.*, vol. 12, pp. 665–669, 2013.

[36] S. K. Podilchak, P. Baccarelli, P. Burghignoli, A. P. Freundorfer, and Y. M. M. Antar, "A sectored planar periodic leaky-wave antenna fed by a printed surface-wave source," *IEEE Antennas Propag. Soc. AP-S Int. Symp.*, pp. 1286–1287, 2014.

[37] J. A. Encinar, "Mode-Matching and Point-Matching Techniques Applied to the Analysis of Metal-Strip-Loaded Dielectric Antennas," *IEEE Trans. Antennas Propag.*, vol. 38, no. 9, pp. 1405–1412, 1990.

[38] P. Burghignoli, P. Baccarelli, F. Frezza, A. Galli, P. Lampariello, and A. A. Oliner, "Low-frequency dispersion features of a new complex mode for a periodic strip grating on a grounded dielectric slab," *IEEE Trans. Microw. Theory Tech.*, vol. 49, no. 2, pp. 2197–2205, 2001.

[39] P. Baccarelli, P. Burghignoli, F. Frezza, A. Galli, P. Lampariello, G. Lovat, and S. Paulotto, "Modal properties of surface and leaky waves propagating at arbitrary angles along a metal strip grating on a grounded slab," *IEEE Trans. Antennas Propag.*, vol. 53, no. 1 I, pp. 36–46, 2005.

[40] M. Nannetti, F. Caminita, and S. Maci, "Leaky-wave based interpretation of the radiation from holographic surfaces," in *IEEE Antennas and Propagation Society, AP-S International Symposium (Digest)*, 2007, pp. 5813–5816.

[41] S. Cakmakyapan, A. E. Serebryannikov, H. Caglayan, and E. Ozbay, "Spoof-plasmon relevant one-way collimation and multiplexing at beaming from a slit in metallic grating.," *Opt. Express*, vol. 20, no. 24, pp. 26636–48, 2012.

[42] H. Caglayan, I. Bulu, and E. Ozbay, "Off-axis beaming from subwavelength apertures," *J. Appl. Phys.*, vol. 104, no. 2008, 2008.

[43] B. H. Fong, J. S. Colburn, J. J. Ottusch, J. L. Visher, and D. F. Sievenpiper, "Scalar and Tensor Holographic Artificial Impedance Surfaces," *IEEE Trans. Antennas Propag.*, vol. 58, no. 10, pp. 3212–3221, Oct. 2010.

[44] G. Minatti, M. Faenzi, E. Martini, F. Caminita, P. De Vita, D. González-ovejero, M. Sabbadini, and S. Maci, "Modulated Metasurface Antennas for Space : Synthesis , Analysis and Realizations," *IEEE Trans. Antennas Propag.*, vol. 63, no. 4, pp. 1288–1300, 2015.

[45] C. J. Vourch and T. D. Drysdale, "Parametric study of a double shifted 'Bull's eye' structure at V-band for beamforming," *2014 Loughbrgh. Antennas Propag. Conf. LAPC 2014*, no. November, pp. 461–464, 2014.

[46] C. J. Vourch and T. D. Drysdale, "V-band Bull's eye antenna for multiple discretely steerable beams," *IET Microwaves, Antennas Propag.*, vol. 10, no. 3, pp. 318–325, 2016.

[47] C. J. Vourch and T. D. Drysdale, "Directivity enhancement of V-band 'Bull's eye' antenna with dielectric superstrate," *2014 Loughbrgh. Antennas Propag. Conf. LAPC 2014*, no. November, pp. 277–280, 2014.

[48] S. Alkaraki, Z. Hu, and Y. Gao, "High gain and steerable Bull's eye millimetre wave antenna," in *Antennas and Propagation USNC/URSI National Radio Science Meeting, 2015 IEEE International Symposium on*, 2015, no. July, pp. 2041–2042.

[49] www.cst.com, "CST Microwave Studio." .

[50] D. Yeop, K.-Y. Jung, and Y. Bae, "Transmission Through an Annular Aperture Surrounded With Corrugations in a PEC Plane," *Antennas Wirel. Propag. Lett. IEEE*, vol. 14, pp. 179–182, 2015.

[51] Y. Hua and T. K. Sarkar, "Generalized Pencil-of-Function Method for Extracting Poles of an EM System from Its Transient Response," *IEEE Transactions on Antennas and Propagation*, vol. 37, no. 2. pp. 229–234, 1989.

[52] M. D. Auria, W. J. Otter, J. Hazell, B. T. W. Gillatt, C. Long-collins, and N. M. Ridler, "3-D Printed Metal-Pipe Rectangular Waveguides," *IEEE Trans. Components, Packag. Manuf. Technol.*, vol. 5, no. 9, pp. 1339–1349, 2015.

Unai Beaskoetxea received the M. Sci. degree in telecommunication engineering, from the Public University of Navarre, Navarre, Spain, in 2013, where he is currently working toward the Ph.D. degree with the advisory of Miguel Beruete. He is currently a Project Assistant with the Antennas Group, Public University of Navarre. His interests include leaky-wave antennas, metamaterials, extraordinary transmission structures, and different research fields in the microwave to infrared range.

Stefano Maci (M'92–SM'99–F'04) is a Professor at the University of Siena, Siena, Italy, and the Director of the Ph.D. School of Information Engineering and Science, which presently includes about 60 Ph.D. students. His research interests include high-frequency and beam representation methods, computational electromagnetics, large phased arrays, planar antennas, reflector antennas and feeds, metamaterials and metasurfaces. His research activity is documented in 10 book chapters, 140 papers published in international journals (among which 80 on IEEE journals) and about 300 papers in proceedings of international conferences. Prof. Maci has been a member of the Technical Advisory Board of 11 international conferences and a member of the Review Board of six international journals, since 2000. He has been responsible for

five projects funded by the European Union (EU). From 2004 to 2007 he was WP leader of the Antenna Center of Excellence (ACE, FP6) and in 2007 he was International Coordinator of a 24-institution consortium of a Marie Curie Action (FP6). He was the Founder of the European School of Antennas (ESoA), a post-graduate school that presently comprises 34 courses on antennas, propagation, electromagnetic theory, and computational electromagnetics, conducted by 150 teachers coming from 15 different countries. He has also been a member of the AdCom of the IEEE Antennas and Propagation Society (IEEE AP-S), an Associate Editor of the IEEE *Trans on Antennas Propagat*, a member of the Italian Committee for Professor Promotion, the Chair of the Award Committee of IEEE AP-S, a member of the Board of Directors of the European Association on Antennas and Propagation (EurAAP), a Distinguished Lecturer of the IEEE Antennas and Propagation Society, a member of the Antennas and Propagation Executive Board of the Institution of Engineering and Technology (IET, U.K.). He is presently the Director of ESoA, a member of the Technical Advisory Board of the URSI Commission B, a member of the Delegate Assembly of EuRAAP, and Director of the FORESEEN center, a consortium of 34 international institutions. He has been recipient of several awards, among which the EurAAP Carrier Award 2014, and other Awards for Best Papers in conferences and journals.

Miguel Navarro-Cía (S'08–M'10–SM'15) was born in Pamplona, Spain, in 1982. He received the M.Sci. and Ph.D. degrees in Telecommunication Engineering, and M.Res. degree in Introduction to Research in Communications from Universidad Pública de Navarra, Navarra, Spain, in 2006, 2010 and 2007, respectively.

From September 2006 to January 2010, and from February 2010 until March 2011, he worked as a Predoctoral Researcher (FPI fellowship recipient) and a Research & Teaching Assistant in the Electrical and Electronic Engineering Department, Universidad Pública de Navarra, respectively. He was a Research Associate at Imperial College London and University College London in 2011 and 2012, respectively, and a Junior Research Fellow at Imperial College London from December 2012 until November 2015. Currently he is Birmingham Fellow in the School of Physics and Astronomy, University of Birmingham. He is also affiliated as a Visiting Researcher with Imperial College London and University College London. He worked as Visiting Researcher at University of Pennsylvania for 3 months in 2010, at Imperial College London in 2008, 2009 and 2010 for 4, 6 and 3 months, respectively, and at Valencia Nanophotonics Technology Center for 2 months in 2008. His current research interests are focused on plasmonics, near-field time-domain spectroscopy/microscopy, metamaterials, antennas and frequency selective surfaces at millimeter-wave, terahertz and infrared.

Dr. Navarro-Cía is a Senior Member of the Optical Society of America, and a Member of the European Association on Antennas and Propagation (EurAAP), and the Spanish National Association and Professional Board of Telecommunication Engineers. He was awarded with the Best Doctoral Thesis in Basic Principles and Technologies of Information and Communications, and Applications corresponding to the XXXI Edition of Awards "Telecommunication Engineers" 2010 and the 2012 CST University Publication Awards to the best international journal publication using CST Microwave Studio™ and was recipient of the 2011 Junior Research Raj Mittra Travel Grant.

Miguel Beruete was born in Pamplona, Spain, in 1978. He received the M.Sci. and Ph.D. degrees in telecommunication engineering, from the Public University of Navarre (UPNA), Navarre, Spain, in 2002 and 2006, respectively.

From September 2002 to January 2007, he was working as Predoctoral Researcher (FPI fellowship recipient) in the Electrical and Electronic Engineering Department, Public University of Navarre. From January to March 2005 he worked as visiting researcher at the University of Seville, as a part of his doctoral research. From February 2007 to September 2009 he was at the electronics department of the technological center CEMITEC in Noain (Navarre), developing, designing and measuring high frequency communication devices. In September 2009 he joined the TERALAB at UPNA, as a post-doc Ramón y Cajal fellow researcher under the supervision of Prof. Mario Sorolla. In March 2014, he joined the Antennas Group-TERALAB of UPNA, where he supervises several Ph.D. and M.Sci. Theses and is responsible of the TERALAB laboratory. Dr. Beruete has authored more than 100 JCR articles, 3 book chapters, 3 patents, near 250 conference communications and acts as a reviewer for more than 40 international journals. His research interests are directed towards terahertz sensing and communication technology, including metamaterials, plasmonics, extraordinary transmission structures, leaky-wave antennas, nanoantennas, and in general quasioptical devices.

Dr. Beruete was awarded the Ph.D. Prize from the Public University of Navarre (2006–2007) for the best Doctoral Thesis in the year 2006–2007, two CST University Publication Awards for the best international journal publication using CST in the years 2005 and 2012, the XII Talgo Award of Technological Innovation in 2011 and several awards in international conferences.